Journal of Alloys and Compounds 688 (2016) 1053–1057

Contents lists available at ScienceDirect

Journal of Alloys and Compounds

journal homepage: http://www.elsevier.com/locate/jalcom

Magnetization process of nanocrystalline mischmetal-Fe-B ribbons

Ming Zhang [a], Yao Liu [a], Zhubai Li [b], Licong Peng [b], Baogen Shen [a, *], Fengxia Hu [b], Jirong Sun [b]

[a] Beijing National Laboratory for Condensed Matter Physics, Institute of Physics, Chinese Academy of Sciences, Beijing, 100190, China
[b] Key Laboratory of Integrated Exploitation of Bayan Obo Multi-Metal Resources, Inner Mongolia University of Science and Technology, Baotou, 014010, China

ARTICLE INFO

Article history:
Received 22 March 2016
Received in revised form
15 June 2016
Accepted 8 July 2016
Available online 9 July 2016

Keywords:
Permanent magnets
Rapid-solidification
Magnetization
Mischmetal

ABSTRACT

Mischmetal-Fe-B ribbons were prepared by melt-spinning method, and industrial mischetal with low purity was selected as the raw material. By introducing La and employing nonequilibrium technology, we successfully avoid the formation of $CeFe_2$ phase, which decreases magnetic performance greatly. Considerable energy product and intrinsic coercivity were achieved in $(MM)_{2.4}Fe_{14}B$, which are 80.69 kJ/m^3 and 500 kA/m, respectively. Phase composition and magnetization process of all the samples were investigated. Strong pinning effect was found in all rare-earth-rich samples and was identified as a crucial factor to obtain high coercivity in ribbons compared with the sintered magnets. The Henkel plot is also measured to investigate the intergrain interaction and the results show a strong exchange coupling between grains. Based on these results, the difference in magnetic performance between nanocrystalline ribbons and sintered magnets can be explained.

1. Introduction

Recently, abundant-rare-earth-based, mainly Ce-based [1–4], permanent magnets have attracted much attention due to the rising price of neodymium. Compared with high Ce-substitution magnets, besides economic consideration, using mischmetal as raw material, also give the advantages in utilizing rare-earth resource in equilibrium and reducing environmental contamination caused by the extraction process. Actually, soon after NdFeB magnet was invented, enormous researches were launched on the mischmetal-based magnets [5–7]. At the very beginning, mischmetals with different components, including some artificial rare earth alloys [7], were used. The results showed that employable permanent magnetic properties can be hardly achieved when the mischmetal contains too much La and/or Ce. Subsequently, the effects of La and Ce in $R_2Fe_{14}B$ magnets on permanent magnetic properties were investigated by substitution approach [8–14], and nonlinear dependence of coercivity, remanence ratio and squareness on the content of La and/or Ce were found [11–14]. Niu et al. prepared the sintered R-Fe-B magnets with high coercivity by using dual alloys method based on mischmetal. They found that the coercivity of magnets first drops rapidly and then decrease slowly with the increase of alloy A. Magnets with the nominal composition of $MM_{15.30}Co_{0.65}Cu_{0.08}B_{6.11}Fe_{bal}$ exhibit a coercicity of 32 kA/m and a remanence ratio of 0.82 [11]. Li et al. investigated the effect of substitution of Ce for Nd in $Nd_{12-x}Ce_xFe_{82}B_6$ nanocrystalline ribbons. Both the coercivity and maximum magnetic energy product were found decreasing linearly until about 2/3 of Nd was substituted by Ce. Further substitution brings about a dramatic drop of permanent magnetic properties [12]. Yan et al. fabricated $(Di_{1-x}Ce_x)_{27.5}Dy_3Al_{0.1}Cu_{0.1}Fe_{bal}B_1$ sintered magnets, and an unusual increase of coercivity was found when Ce account for 1/4 of the rare earth [13]. This abnormal phenomenon was also found in $(Nd_{1-x}Ce_x)_2Fe_{14}B$ melt spun ribbons by Pathak et al. [14]. Fig. 1 shows the dependence of coercivity on the La and/or Ce containing in the works mentioned above.

These previous studies provide much useful information about the effect of La and/or Ce substitution on the structure sensitive properties, such as coercitity, remanence ratio and squareness. These investigations also reveal the feasible percentage of La and/or Ce, which is about 30% or less, and the permanent magnetic properties of crude-mischmetal-based magnets are relatively low. Further more, the coercivity mechanism and intergrain interaction effect are still not very clear yet, which also hinders the fabrication of high performance mischmetal-based magnets. Therefore, to synthesize $R_2Fe_{14}B$-type magnets using industrial mischmetal with

* Corresponding author.
E-mail address: shenbg@iphy.ac.cn (B. Shen).

http://dx.doi.org/10.1016/j.jallcom.2016.07.098
0925-8388/

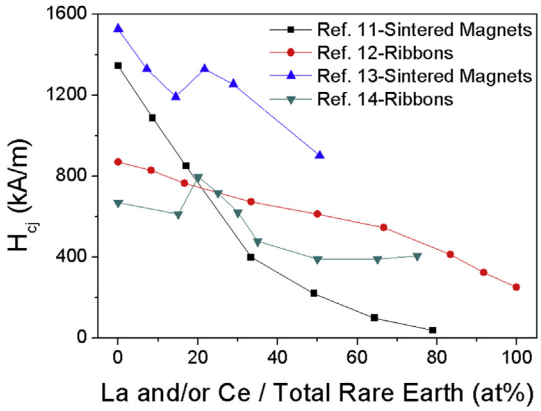

Fig. 1. The dependence of intrinsic coercivity, H_{cj} on La and/or Ce content in reference 11 to 14.

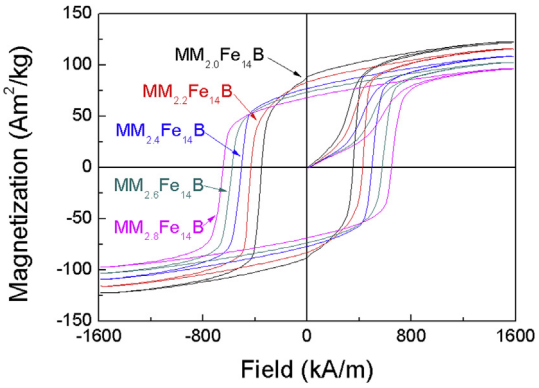

Fig. 2. The hysteresis loops of $(MM)_xFe_{14}B$ ribbons.

Table 1
Contents and impurities of the Mischmetal used in this experiment.

RE	La/RE	Ce/RE	Pr/RE	Nd/RE	Sm/RE	Fe	Si	Mg	W	Zn,Cu,Ti,Ca,Pb,C	Mo	Cr
98.50	28.38	50.66	5.24	15.72	<0.050	0.037	0.016	0.057	0.010	<0.010	0.007	<0.030

impurities and study the permanent magnetic properties are of high significance for both basic researches and practical applications.

In this work, we used the industrial mischmetal extracted from Bastnaesite ore as raw materials and prepared $(MM)_xFe_{14}B$ (MM = mischmetal) ribbons by using melt-spinning technique. Here, we report the phase composition, room-temperature magnetic properties, coercivity mechanism and intergranular interaction of $(MM)_xFe_{14}B$ ribbons.

2. Experimental

The $(MM)_xFe_{14}B$ ingots with x = 2.0, 2.2, 2.4, 2.6 and 2.8 were prepared by arc melting technique in an argon atmosphere of high purity. The purity of starting materials is 99.9% for Fe and 96% for Fe-B alloys. Mischmetal, extracted from bastnaesite with natural element percentage, containing about 28.38 wt% La, 50.66 wt% Ce, 5.24 wt% Pr, and 15.72 wt% Nd with a purity of 98.50% was used in this experiment. Table 1 lists its content of elements in weight percentage. MM was used as the abbreviation of this alloy in chemical formula in the mischmetal. The ribbons were obtained by using melt spinning method with a surface velocity in a range of 10–30 m/s. X-ray diffraction measurements were performed using Cu Kα radiation to determine the crystal structure. The measuring step is 0.02°, and counting time is 2 s per step. The data was analyzed by using GSAS. Topographic and magnetic domain images were obtained by Lorentz transmission electron microscope (Lorentz TEM). Room temperature magnetic properties were measured by vibrating sample magnetometer (VSM) with a maximum magnetic field of 1600 kA/m. The applied field is parallel to the face of ribbons and no demagnetization correction for the geometry of the sample was made, because the demagnetization factor is nearly 1.

3. Results and discussion

The permanent magnetic properties of ribbons prepared by melt-spinning technique strongly dependents on the wheel velocity. Fig. 2 shows the initial magnetization curves and hysteresis loops of $(MM)_xFe_{14}B$ ribbons prepared at the optimum wheel velocity of 20 m/s. The values of remanence B_r, H_{cj}, $(BH)_{max}$, remanence ratio and squareness (which is defined by the ratio of the integral $\int_{-H_c}^{0} MdH$ to $M_r{}^*H_{cj}$) were listed in Table 2. With an increase of rare earth content, both the saturation magnetization and remanence decrease due to the formation of paramagnetic rare-earth-rich phases. Meanwhile, the intrinsic coercivity enhances. The $(BH)_{max}$ increases at first and attains to the maximum of 80.69 kJ/m^3 at x = 2.4, and then decreases. The magnetic properties of these ribbons are much better than the sintered magnets containing about 80% La and Ce due to the specific phase

Table 2
Room-temperature magnetic properties of $(MM)_xFe_{14}B$ ribbons.

Samples	B_r T	H_{cj} kA/m	$(BH)_{max}$ kJ/m^3	Remanence ratio	Squareness
$(MM)_{2.0}Fe_{14}B$	0.828	352	76.95	0.72	0.74
$(MM)_{2.2}Fe_{14}B$	0.783	427	80.37	0.72	0.76
$(MM)_{2.4}Fe_{14}B$	0.727	500	80.69	0.71	0.82
$(MM)_{2.6}Fe_{14}B$	0.693	578	75.36	0.72	0.79
$(MM)_{2.8}Fe_{14}B$	0.644	648	66.69	0.71	0.80

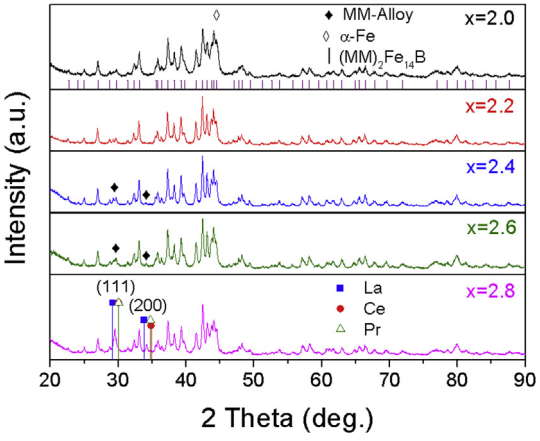

Fig. 3. The XRD patterns of $(MM)_xFe_{14}B$ ribbons.

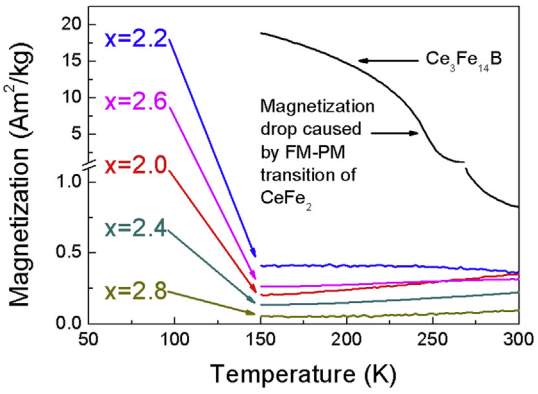

Fig. 4. The dependence of magnetization on temperature of $Ce_3Fe_{14}B$ and $(MM)_xFe_{14}B$.

composition and microstructure.

X-ray diffraction patterns, shown in Fig. 3, indicate that the main phase crystallizes in $R_2Fe_{14}B$ structure, and no RE-Fe binary phases or rare earth oxides was found for all samples. In consideration of the resolution limit of XRD technique, the absence of $CeFe_2$ was double-checked by measuring the dependence of magnetization on temperature under a low field of 8 kA/m, meanwhile, $Ce_3Fe_{14}B$ ribbon was used as the contrast. From Fig. 4, we can see the existence of $CeFe_2$ brings about an obvious drop in magnetization at its Curie temperature in the $Ce_3Fe_{14}B$ ribbon, but no such drop was found in the $(MM)_xFe_{14}B$ ribbons. The phase composition is one of the key factors in high Ce-containing magnets, and mischmetal used in our experiment contains about 50% Ce. Early investigations showed that a second-phase of $CeFe_2$ can hardly be excluded in this kind of magnets. In Herbst's experiment, $Ce_3Fe_{14}B$ ribbons contain about 12% of $CeFe_2$ [1]. Niu et al. declared that the formation of $CeFe_2$ implies low coercivity in high Ce-containing sintered R-Fe-B magnets [11]. Our previous study revealed that the incorporation of La can hinder the formation of $CeFe_2$ in (La,Ce)-Fe-B ribbons [15]. However, soon after this discovery, we noted that the addition of La might be able to restrain the $CeFe_2$ formation only in melt spinning process. In Ref. [11], the raw material mischmetal also contains La, and the atomic ratio of La to Ce is almost the same compared to the La-Ce mischmetal we used in our previous work, but $CeFe_2$ was also found in the sintered magnets. It means that $CeFe_2$ cannot be avoided merely by La addition. The absence of $CeFe_2$ in $(MM)_xFe_{14}B$ ribbons in our work indicates that nonequilibrium technology can also impede the formation of $CeFe_2$. Except 2:14:1 phase diffraction, two peaks located at 29.5° and 34.2° appear for the sample with $x = 2.4$ in the XRD patterns, and grow with the content of mischmetal. These peaks indicated the existence of secondary phase. We noticed that, the diffraction peaks of (111) and (200) of La, Ce, Pr with a space group of *Fm*-3*m* locate around these two peaks. Hence, the secondary phase should be La-Ce-Pr solid solution.

The grain size calculated by Scherrer equation based on the x-ray diffraction pattern is about 35 nm. A direct observation was carried out by using Lorentz TEM. Fig. 5 revealed the topographic image (a) and magnetic domain images of $(MM)_{2.2}Fe_{14}B$. We obtained under focused (b), in focused (c) (without magnetic information), and over focused (d) image respectively, the red points marked the same location in different images. It can be seeing from the images, that the size of magnetic domain is as large as, or larger than the size of grain, and the domain wall located on the grain boundary. Other samples share a similar presentation.

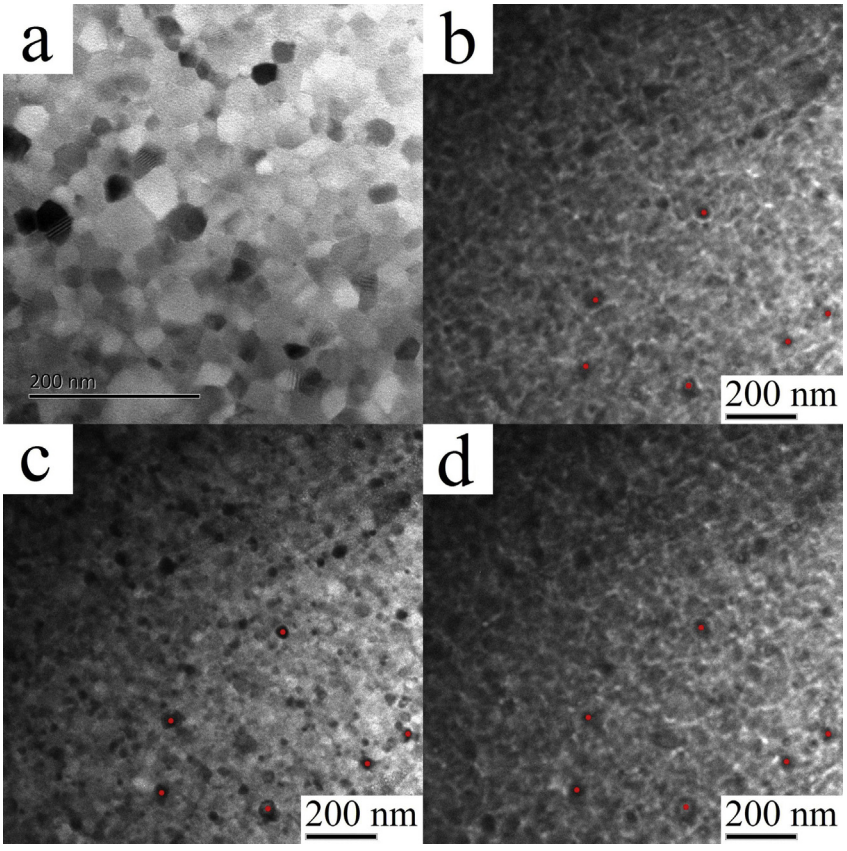

Fig. 5. The topographic images (a) (c) and magnetic domain images (b) (d) of $(MM)_{2.2}Fe_{14}B$.

As shown in Fig. 2, the magnetization in the initial magnetization curve increases slowly until the applied field approach the intrinsic coercivity, which shown a characteristic of pinning mechanism. More details can be given by the field dependence of normalized coercivity and normalized remanence derived from minor loops, shown in Fig. 6. Usually, in practical cases, the shape of plots can hardly match a single coercivity mechanism model, neither pinning nor nucleation. According to general viewpoint, if the normalized coercivity increase faster than the remanence with the external field, the magnetization reversal is deemed to be mainly governed by domain wall pinning effect, otherwise, it is the domain nucleation dominant the magnetization reversal process [16]. In this experiment, the coercivity increase faster than remanence for all samples. As the increase of rare earth content, the gap between two curves becomes wider which indicates the pinning effect is stronger in rare earth rich samples. As mentioned previously, the excess rare earth crystallizes in a secondary phase. Therefore, this phase is supposed to be one of the pinning centers.

Fig. 7 shows the irreversible susceptibility χ_{irr}/M_s vs. normalized demagnetization field H/H_{cj}. The inset shows the distribution of irreversible susceptibility more than 0.2 times of the maximum value. As the increase of mischmetal content, the distribution of irreversible susceptibility centralized on the H/H_{cj}. A narrow distribution of irreversible susceptibility related to a more uniform magnetization reversal process. The $(MM)_{2.0}Fe_{14}B$ ribbon contains a small amount of α-Fe due to the loss of rare earth metal during the arc melting process. The existence of intergranular α-Fe layers increased the saturation magnetization, but the magnetization reversal becomes more non-uniform [17].

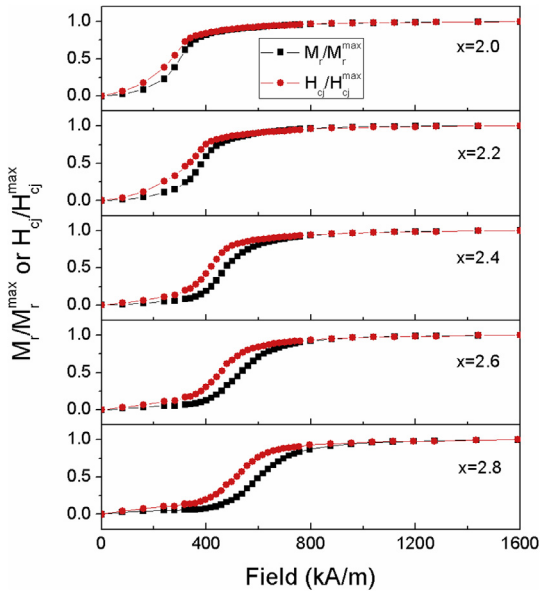

Fig. 6. The dependence of M, and H_c on applied field in minor loops of $(MM)_xFe_{14}B$ ribbons.

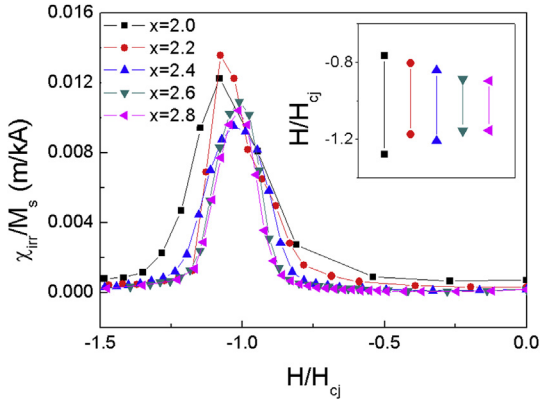

Fig. 7. The irreversible susceptibility vs. normalized demagnetizing field. The inset is the distribution of irreversible susceptibility.

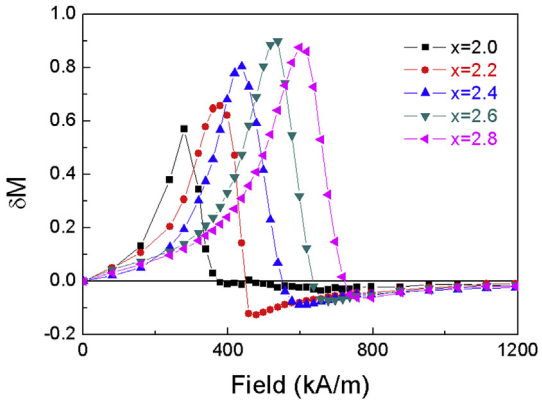

Fig. 8. The Henkel plots of $(MM)_xFe_{14}B$ ribbons.

As shown in Table 2, the remanence ratio M_r/M_s of the $(MM)_xFe_{14}B$ ribbon ranges from 0.71 to 0.72. A value of M_r/M_s larger than 0.5 indicates the existence of intergranular exchange coupling in isotropic magnet composed of uniaxial anisotropy single-domain grains. The δM which defined as $\delta M(H) = I_d(H) - [1 - 2I_r(H)]$ is normally used to evaluate the intergranular exchange coupling [18–20], where $I_d(H)$ is the normalized dc-demagnetization remanence as a function of the reversal field, and $I_r(H)$ is the normalized initial isothermal remanence as a function of the applied field. A positive value of δM means the exchange coupling is dominant over magnetostatic (dipolar) interaction. Fig. 8 shows the δM curves of $(MM)_xFe_{14}B$ ribbons. All the samples reveal positive peaks around their coercivity, but vary in values. $(MM)_{2.0}Fe_{14}B$ ribbon possesses the lowest maximum value of δM among all the samples. It means that the intergranular exchange coupling is weak, and the magnetization reversal process is relatively non-uniform caused by the existence of intergranular α-Fe layers. In the $(MM)_{2.2}Fe_{14}B$ ribbons, there should form a thin layer of rare earth phase between the main phase grains with the increase of rare earth concentration, and the grain boundary becomes smooth, hence the maximum value of δM increase due to the improvement of grain boundaries [15,17]. As rare earth content increases further, the peak value of δM increases and the valley value of δM decreases simultaneously. $(MM)_{2.6}Fe_{14}B$ and $(MM)_{2.8}Fe_{14}B$ ribbons possess almost the same maximum value of δM, and their minimum values are all approaching zero.

4. Conclusions

In summary, high performance $(MM)_xFe_{14}B$ ribbons, free of Tb and Dy, have been fabricated by using melt-spinning method. Industrial mischmetal contains about 80% La and Ce was used as the raw material. The results suggest that mischmetal-based magnets with great properties can be obtained by using nonequilibrium process. Detailed analysis of the magnetization process indicates that the domain wall pinning effect is obvious in all rare-earth-rich samples during the magnetization reversal process. The strong of domain wall pinning effect should be the primary cause of the

higher coercivity in ribbons compared to the sintered magnets. The intergranular interaction and its contribution to the enhancement of remanence and squareness were studied, strong exchange coupling was found in all rare-earth-rich samples. The contribution of this article is not limited to the fabrication of high performance mischmetal-Fe-B ribbons successfully, what is more is the analysis guides the new approach to obtain practical mischmetal based magnets.

Acknowledgements

This work was supported by the National Basic Research Program of China (Grant No. 2014CB643702).

References

[1] J.F. Herbst, M.S. Meyer, F.E. Pinkerton, J. Appl. Phys. 111 (2012) 07A718.
[2] E.J. Skoug, M.S. Meyer, F.E. Pinkerton, M.M. Tessema, D. Haddad, J.F. Herbst, J. Alloys Comp. 574 (2013) 552–555.
[3] C.J. Yan, S. Guo, R.J. Chen, D. Lee, A. Yan, IEEE Trans. Mang. 50 (2014) 2104604.
[4] C. Zhou, K. Sun, F.E. Pinkerton, M.J. Kramer, J. Appl. Phys. 117 (2015) 17A714.
[5] W. Gong, G.C. Hadjipanayis, J. Appl. Phys. 63 (1988) 3513.
[6] M. Tanimoto, K. Honda, J. Yamasaki, K. Mohri, O. Kohmoto, IEEE Trans. Mang. Jpn. 3 (1988) 428–429.
[7] S.X. Zhou, Y.G. Wang, R. H/Oier, J. Appl. Phys. 75 (1994) 6268.
[8] A. Alam, M. Khan, R.W. McCallum, D.D. Johnson, Appl. Phys. Lett. 102 (2013) 042402.
[9] H.W. Chang, C.H. Chen, C.C. Hsieh, W.C. Chang, J. Nanosci. Nanotechnol. 11 (2011) 2756–2760.
[10] H.W. Chang, J.Y. Gan, C.W. Shih, C.C. Hsieh, W.C. Chang, C.C. Shaw, IEEE Trans. Mang. 50 (2014) 2100904.
[11] E. Niu, Z.A. Chen, G.A. Chen, Y.G. Zhao, J. Zhang, X.L. Rao, B.P. Hu, Z.X. Wang, J. Appl. Phys. 115 (2014) 113912.
[12] Z.B. Li, B.G. Shen, M. Zhang, F.X. Hu, J.R. Sun, J. Alloys Comp. 628 (2015) 325–328.
[13] C.J. Yan, S. Guo, R.J. Chen, D. Lee, A. Yan, IEEE Trans. Mang. 50 (2014) 2102605.
[14] A.K. Pathak, M. Khan, K.A. Gschneidner Jr., R.W. McCallum, L. Zhou, K. Sun, K.W. Dennis, C. Zhou, F.E. Pinkerton, M.J. Kramer, V.K. Pecharsky, Adv. Mater. 27 (2015) 2663–2667.
[15] M. Zhang, Z. Li, F. Hu, B. shen, J. Sun, J. Alloys Comp. 651 (2015) 144–148.
[16] K.H.J. Buschow, Rep. Nog. Phys. 54 (1991) 1123.
[17] Z.B. Li, M. Zhang, B.G. Shen, J.R. Sun, Appl. Phys. Lett. 102 (2013) 102405.
[18] P.E. Wohlfarth, J. Appl. Phys. 29 (1958) 595.
[19] O. Henkel, Phys. Status Solidi 7 (1964) 919.
[20] P.E. Kelly, K. O'Grady, P.I. Mayo, R.W. Chantrell, IEEE Trans. Magn. 25 (1989) 3881.